Stark deceleration and trapping of hydrogen Rydberg atoms

E. Vliegen, S. D. Hogan, H. Schmutz, and F. Merkt*
Laboratorium für Physikalische Chemie, ETH Zürich, CH-8093 Zurich, Switzerland
(Received 7 March 2007; published 10 August 2007)

Hydrogen atoms in supersonic expansions with velocities in the range from 700 to 800 m/s have been excited to Rydberg-Stark states with principal quantum number n between 20 and 40, decelerated to zero velocity in the lab frame using time-dependent inhomogeneous electric fields, and trapped in a two-dimensional electrostatic trap with an initial density of $\approx 5\times 10^6$ cm^{-3}. The motion of the atomic cloud in the trap was observed by measuring the times of flight and images of the H^+ ions produced by pulsed field ionization. The velocity distribution of the trapped atoms can be described by an effective temperature of 350 mK. The decay of the population of trapped atoms does not follow a single-exponential behavior and has contributions from radiative and collisional processes.

DOI: 10.1103/PhysRevA.76.023405 PACS number(s): 33.80.Ps, 32.60.+i, 32.80.Rm, 39.10.+j

I. INTRODUCTION

Much effort has recently been invested in studies of cold Rydberg gases. Because of the large dipole-dipole interactions between Rydberg atoms, cold Rydberg gases provide ideal systems with which to study many-body effects in dilute samples [1–3], to investigate the evolution from dense, cold Rydberg clouds into cold plasmas [4,5], and may offer unique advantages for quantum information processing [6]. Trapped cold Rydberg atoms and molecules are also ideal samples for spectroscopic experiments. Not only is the Doppler width reduced because of the low mean velocity but also the interaction times can be much longer than in a typical molecular-beam experiment, resulting in the possibility to study Rydberg states with very high spectral resolution.

Two approaches can be followed to generate (ultra)cold Rydberg gases at rest in the laboratory frame. The first method, which is so far the only one to have been realized experimentally, involves the excitation of atoms stored in a magneto-optical trap (MOT) to high Rydberg states [1–5,7]. This method, however, is restricted to a very limited range of atoms, primarily alkali-metal atoms.

The second method, which is in principle applicable to all atoms and molecules in the gas phase, was proposed 25 years ago [8,9], but to date has not yet been realized experimentally. It involves slowing and trapping Rydberg atoms using inhomogeneous electric fields. Progress has been made recently in the control of the translational motion of Rydberg atoms and molecules with inhomogeneous electric fields [10–14] and Rydberg atoms in supersonic beams have been stopped [15].

We demonstrate here the operational principle of a two-dimensional electrostatic Rydberg atom trap, characterize its properties, and present its application to trapping H atoms in Rydberg states of principal quantum number between $n=20$ and 40. The experiments rely on the large dipole moments exhibited by Rydberg-Stark states, which amount to $\frac{3}{2}a_0enk$, where a_0, e, and k are the Bohr radius, the elementary charge, and the difference between the parabolic quantum numbers n_1 and n_2 [16], respectively. At $n=20$, the dipole moment can be three orders of magnitude larger than in typical polar molecules in their ground or low valence electronic states. Large forces can thus be exerted on Rydberg atoms and molecules using inhomogeneous electric fields.

II. EXPERIMENT

The experimental setup and excitation scheme used in this work are identical to those used in our previous studies [14,15]. The hydrogen atoms are produced by 193-nm excimer laser photolysis of NH_3, seeded in argon, in a quartz capillary located at the exit of a pulsed nozzle. The supersonic beam containing the H atoms passes a skimmer after which the H atoms are photoexcited to Rydberg-Stark states via the $2\ ^2P$ state using a resonant two-photon excitation scheme. The two counterpropagating laser beams cross the supersonic beam at right angles. The photoexcited hydrogen atoms initially move at a velocity of $\approx$750 m/s in the positive z direction and have a longitudinal temperature of 0.1 K [see Fig. 1(b) for the definition of the axes]. The velocity distribution in the y dimension is centered around zero with a temperature that is determined by the size of the laser beams and is approximately equal to 2.3 mK. The spatial distributions of the Rydberg particles in the y and z dimensions can be approximated by a Gaussian with a full width at half maximum of 0.8 mm.

The Rydberg atoms are decelerated and trapped using the voltage pulse sequence and electrode setup displayed in Fig. 1. The pulse sequence consists of four parts: photoexcitation ($t=0$), deceleration ($0<t<10$ μs), trapping (10 μs $<t<t_{\mathrm{PFI}}$), and field ionization (t_{PFI}). The electric-field strength distributions for typical voltages during deceleration and trapping are shown in Figs. 1(b) and 1(c), respectively. At photoexcitation, the potentials on electrodes 1 and 2 are set to $V_1=-V_2=V_{\mathrm{trap}}^{12}$, and the potentials on electrodes 3 and 4 to $-V_3=V_4=V_{\mathrm{trap}}^{34}$. V_{trap}^{12} is chosen so that the different Stark states of a given n manifold can be prepared optically with a high selectivity. After photoexcitation, the particles are decelerated by switching the potentials $-V_3=V_4$ to a high voltage, $|V_3|=|V_4|=V_{\mathrm{decel}}$, which decays exponentially to V_{trap}^{34}

*Corresponding author.

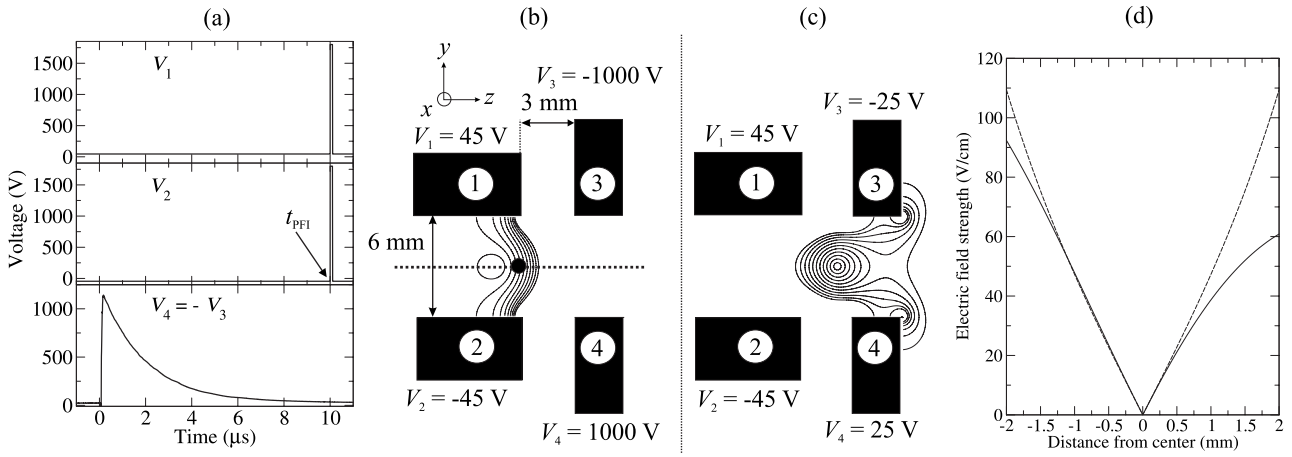

FIG. 1. (a) Voltage pulse sequence applied to the four electrodes. Photoexcitation takes place at $t=0$ and pulsed field ionization takes place at t_{PFI}. (b) Schematic view of the electrode setup during deceleration. The particles, which move along the z axis, are excited at the position indicated by the black dot and are decelerated because of the large electric field inhomogeneity. (c) Schematic view of the electrode setup during trapping. The solid lines in (b) and (c) are lines of constant electric-field strength in steps of 100 V/cm (b) and 10 V/cm (c). (d) Electric-field strength along the z axis (solid line) and along the y axis (dashed line) about the center of the trap.

with a $1/e$ decay time of 1.9 μs, as described in Ref. [13]. The atoms excited to blueshifted, low-field-seeking Stark states decelerate because they experience an increasing electric-field strength as they fly through the deceleration setup. The time constant and V_{decel} are chosen such that the atoms are at rest in the center of the trap after 10 μs.

The electrode setup with trapping potentials V_{trap}^{12} and V_{trap}^{34} constitutes a two-dimensional trap for atoms in low-field-seeking states because the electric-field strength is zero at the center of the trap and increases in all directions in the yz plane [see Figs. 1(c) and 1(d)]. The field is homogeneous in the x dimension and the velocities of the particles in this dimension, which can be approximated by a temperature in the range from 50 to 100 mK depending on the expansion conditions, do not change during deceleration and trapping.

The hydrogen atoms are finally detected by pulsed field ionization (PFI) using a large positive potential V_{PFI} of 2000 V and of 100 ns duration applied on the first two electrodes after a controllable delay t_{PFI}. The resulting ions are detected on a microchannel plate (MCP) detector where their times of flight (TOF) are recorded. The ion TOF spectra can be directly correlated to the positions of the parent Rydberg atoms along the z axis at the moment of field ionization because the potential differences experienced by the ions, and thus their TOF, depend on their initial positions. The motion of the Rydberg atom cloud within the trap can therefore be reconstructed by analyzing the evolution of the average ion TOF as a function of t_{PFI}. The MCP detector is connected to a phosphor screen behind which a charge-coupled device (CCD) camera is located. Images of the H^+ ion cloud impinging on the MCP detector can be recorded simultaneously with the TOF spectra. The same detection system can also be used to measure the TOF distributions and record images of the neutral Rydberg atoms as described in detail in Ref. [17].

III. RESULTS AND DISCUSSION

A. Trapping times, lifetimes, and trap losses

Figure 2 (a) shows three sets of measurements of the integrated ion signal recorded as a function of ionization delay at different nozzle stagnation pressures. These measurements were made by varying t_{PFI} up to 250 μs in steps of 2 μs and measuring the integrated ion intensity at each time step. In these measurements, the particles were excited to the $n=35$, $k=30$, $|m|=0,2$ Stark states using $V_{trap}^{12}=21$ V. The atoms were subsequently decelerated using $V_{decel}=980$ V, trapped using $V_{trap}^{34}=14$ V, and finally field ionized with $V_{PFI}=2.0$ kV. Under these conditions the lowest saddle point of

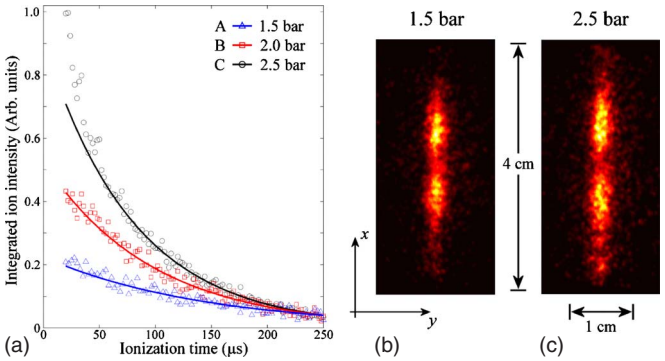

FIG. 2. (Color online) (a) Integrated H^+ ion intensity measured as a function of the delay time between photoexcitation and pulsed field ionization. The initial velocity of the H atoms amounted to 800 m/s. The nozzle stagnation pressure in the measurements was 1.5 bar (trace A), 2.0 bar (trace B), and 2.5 bar (trace C). The traces have been normalized so that the signal strengths are the same for all traces at 250 μs. (b) and (c) CCD camera images of an undecelerated beam of Rydberg hydrogen atoms hitting the MCP. The nozzle stagnation pressure in these two measurements was 1.5 bar (b) and 2.5 bar (c).

the trap lies 38 V/cm above the electric-field strength minimum. This corresponds to a trap depth of 2.6 cm^{-1} for Rydberg atoms with $n=35$ and $k=30$. In the measurements of trace A the nozzle stagnation pressure was 1.5 bar. A single exponential decay, represented by the solid line, with a $1/e$ time constant of 145 μs can be fitted to the data from $t_{PFI}=75$ μs to 250 μs. This curve also reproduces the behavior of the data at times shorter than 75 μs. The initial Rydberg atom density in the trap is estimated from the known trap volume to be $\approx 5\times 10^6$ cm^{-3} by comparing the field ionization signal to the signal of a single ion at the MCP detector.

To obtain the data of trace B and trace C, the nozzle stagnation pressure was increased to 2.0 and 2.5 bar, respectively, while the mean velocity of the atoms in the z dimension was held constant by controlling both the delay time between the excimer and vacuum ultraviolet laser pulses and the arrival time of the neutral undecelerated Rydberg atoms at the MCP detector. Increasing the nozzle stagnation pressure in this way has two effects on the gas beam: (i) the pressure in the gas beam increases and thus the number density of argon atoms and of excited hydrogen atoms increases leading to more collisions, and (ii) the velocities of the excited atoms in the y dimension and in the untrapped x dimension increase. Panels of Figs. 2(b) and 2(c) show two CCD camera images of an undecelerated atomic beam of Rydberg atoms impinging on the MCP 255 μs after excitation. In recording these images, the nozzle stagnation pressure was 1.5 and 2.5 bars, respectively. From these two images, and further images (not shown) recorded at different nozzle stagnation pressures, one sees that the H atoms tend to be located close to the surface of the gas expansion cone and that both the mean velocity and the velocity spread of the excited hydrogen atoms increase with nozzle stagnation pressure. When the Rydberg atoms were ionized 1 μs after excitation we also observed a similar separation of the atomic beam into two parts in the x dimension (see Fig. 4 of Ref. [15]). This behavior is therefore a property of the gas beam and not an effect which occurs between the preparation of the Rydberg states and their detection. The information contained in these images can be reduced to two parameters: the most probable transverse velocity in the x dimension v_{mp}, corresponding to the peak intensities of both lobes of the images, and the velocity v_{hm} corresponding to the points where the intensity has decreased to half its maximal value at the outer edges of the gas expansion cone. The values extracted from the images for the three stagnation pressures used to record the traces in Fig. 2(a) are listed in Table I. A single exponential can also be fitted to the data presented in traces B and C between $t_{PFI}=75$ μs and $t_{PFI}=250$ μs yielding $1/e$ decay times of 100 and 80 μs, respectively. The exponential function fits the data at times shorter than $t_{PFI}=75$ μs for trace B reasonably well, but not for trace C, for which the decay is faster at shorter times.

We attribute the shorter $1/e$ decay times at higher pressure in part to the increased velocity of the atoms in the x dimension. Indeed, the atoms having the largest velocities along the x dimension do not reach the detector. In order to correct for this purely instrumental source of signal loss at longer times, an instrument function was derived from the images recorded for undecelerated beams and the data summarized in Table I. We have assumed the same linear expansion of the atom cloud in the x dimension for the trapping experiments shown in Fig. 2(a) and the free-flight experiments displayed in Figs. 2(b) and 2(c). In the trapping experiments, geometric constraints imposed by the size of the MCP detector and the ion optics restrict the detection to particles which are located less than 0.625 cm away from the beam axis in x dimension. Under these conditions, the instrumental detection functions depicted in Fig. 3(a) are obtained. The effective decay curves of the trapped Rydberg population can be derived by dividing the experimental signal decay curves of Fig. 2(a) with the corresponding instrumental functions and are displayed in Fig. 3(b). The analysis of these curves, which represent our best estimate of the trap losses, lead to the following conclusions:

(i) The measurements at the lower stagnation pressures (1.5 and 2.0 bar) can be fitted well with exponentially decay-

TABLE I. Transverse velocity characteristics of the H atoms in the x dimension of the supersonic expansion extracted from the images recorded for undecelerated beams at nozzle stagnation pressures of 1.5, 2.0, and 2.5 bar. The second column lists the most probable velocities v_{mp} and the third column the velocities v_{hm} at the points where the intensity in the image has decreased to half its maximal value.

Nozzle stagnation pressure	$\lvert v_{mp}\rvert$	$\lvert v_{hm}\rvert$
1.5 bar	13 m/s	26 m/s
2.0 bar	16 m/s	33 m/s
2.5 bar	18 m/s	36 m/s

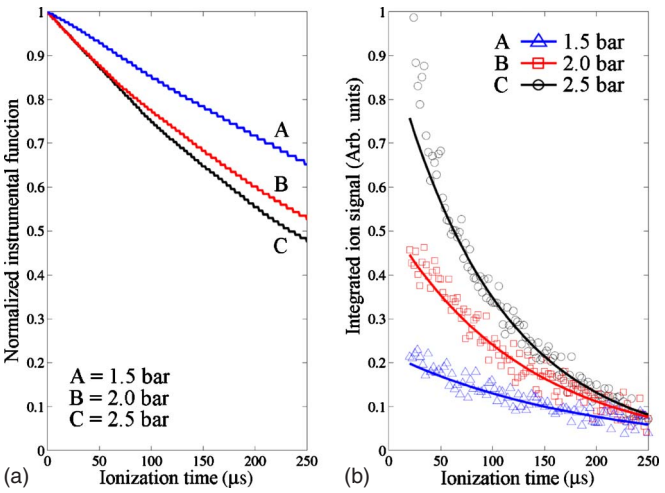

FIG. 3. (Color online) (a) Instrumental function describing the signal losses originating purely from geometrical constraints imposed by the size of the MCP detector and the ion optics for nozzle stagnation pressures of 1.5 bar (trace A), 2.0 bar (trace B), and 2.5 bars (trace C). The steps in the instrumental function are a consequence of the pixels of the CCD camera. (b) Best estimates of the trap losses obtained by dividing the observed signal decay curves with the instrumental function. The solid lines represent single-exponential fits of the data points beyond 75 μs.

ing functions with $1/e$ times of 190 and 130 μs, respectively, represented by solid lines in the figure. A slight deviation indicating a faster decay at the shortest times is recognizable.

(ii) This deviation from a single-exponential decay at short times becomes pronounced in the measurement made at a nozzle stagnation pressure of 2.5 bar. In this case, the trap losses beyond 75 μs can, nevertheless, be described well by an exponential decay function with a $1/e$ decay time of 105 μs.

(iii) The $1/e$ decay times extracted for the three traces of Fig. 3(b) at times longer than 75 μs become faster at increasing nozzle stagnation pressure which indicates the importance of losses by collisional processes. The velocity components of the trapped H atoms along the x dimension of typically 25 m/s (see Table I) is such that these atoms have moved about 1.8 mm away from the beam axis in 75 μs. Collisions with the trailing part of the gas pulse are negligible in this region, and we attribute the decrease in the $1/e$ decay times observed at increasing nozzle stagnation pressures to collisions with the thermalized gas surrounding the gas jet.

(iv) The $1/e$ decay time of the measurement carried out at a 1.5 bar stagnation pressure represents a lower limit of the natural lifetime of the trapped Rydberg atoms. This lifetime is limited either by fluorescence to lower n states that are not trapped, primarily the $n=1$ ground state, or by transitions induced by blackbody radiation. The fluorescence lifetime of the $n=35$, $k=30$, $m=0$ Stark state can be estimated from the values listed in Table 15 of Ref. [18] to be equal to ≈ 150 μs assuming conservation of the magnetic quantum number m. A partial redistribution of m during deceleration and trapping will have the effect of increasing the lifetime, a lifetime of 350 μs being adequate to describe a situation in which m has become completely randomized at $n=35$. The decay by fluorescence thus closely matches the observed trap losses measured in the experiments carried out at the lowest stagnation pressure.

(v) Blackbody radiation certainly also induces transitions and a partial redistribution of the initially prepared Rydberg atom population to states of different n and k values [19]. The time constant associated with all single quantum transitions to neighboring n and k states can be estimated to be ≈ 60 μs at $n=35$ from the expressions listed in Ref. [16]. These transitions induced by blackbody radiation greatly favor small n and k changes and therefore do not cause significant trap losses under our experimental conditions; our trap has indeed a broad acceptance of k and n states (see below).

(vi) The faster decay observed at short times ($\leqslant 75$ μs) and which becomes increasingly noticeable in the measurements carried out at higher nozzle stagnation pressures in Fig. 3(b) can be attributed to collisions of the Rydberg atoms located close to the beam propagation axis where the density of undecelerated argon atoms in the trailing part of the gas pulse is high. These atoms knock the H Rydberg atoms out of the trap. Because of the expansion of the trapped atom cloud in the x dimension discussed above, the H atoms leave the region where the supersonic beam propagates within ≈ 75 μs. Moreover, the intense part of the gas beam has passed the trap after ≈ 50 μs so that collisions with the trailing part of the gas pulse become negligible beyond 75 μs.

B. Temperatures of the atoms in the trap

The time dependence of the velocity and spatial distributions of the trapped atoms decelerated from an initial velocity of 700 m/s were studied for $n=27$, $k=20$, $m=0,2$ Stark states. These distributions can be quantified by comparing the experimental TOF distributions of the ions produced by PFI with the results of trajectory simulations of the Rydberg atoms in the trap and the H^+ ions from the moment of PFI to their arrival at the detector as described in Ref. [13]. We begin this subsection with a qualitative description of the temperature of the atom cloud after the phase-space distribution has reached equilibrium in the trap. We then discuss the evolution of the phase-space distribution at short times.

When the cloud is initially stopped at the center of the trap, the velocity distribution of the trapped atoms in each dimension (z and y) does not correspond to a Maxwell-Boltzmann distribution, but the widths of the distributions correspond to an effective temperature of 350 mK in each dimension. The final temperature is, in this case, determined by the initial size of the trapped atom cloud (diameter 1 mm) and the linear dependence of the electric field on the distance from the center of the trap: The average electric field experienced by the cloud of atoms is 15 V/cm, corresponding to an average potential energy for the $n=27$, $k=20$ Stark state of 0.52 cm^{-1}. Because $E_{kin}=\frac{1}{2}E_{pot}$ in a linear trap, the average kinetic energy is 0.26 cm^{-1} which corresponds to a temperature of 370 mK, approximately equal to the temperature of 350 mK derived from the simulations. The temperature does not depend critically on the initial temperature of the atom cloud nor on its dimensions but is determined by the field distribution in the trap.

When the trapped atoms are initially located off center, the final temperature is primarily determined by the position of the atom cloud at the end of the deceleration period. The further away from the center of the trap the cloud is stopped, the higher the final temperature, reflecting the higher potential energy.

The dynamics in the z dimension of the trapped Rydberg atom cloud were studied for several initial conditions by recording the ion TOF distributions as a function of t_{PFI}. The principle of the measurements is illustrated in Fig. 4(a) which displays three ion TOF spectra recorded immediately after the deceleration period using three different deceleration voltages. For $V_{decel}=1155$ V, the atom cloud is located close to the center of the trap at the end of the deceleration, and the TOF spectrum peaks at ≈ 550 ns (full line). For a larger (smaller) deceleration voltage of 1375 V (935 V), the maximum of the TOF distribution shifts to shorter (longer) times [see dotted (dashed) line in Fig. 4(a)] because the atom cloud is located before (after) the center of the trap at the end of the deceleration period and the ions experience a larger (smaller) extraction potential.

Figures 4(b) and 4(c) of display the average ion TOF obtained from the experimental and simulated ion TOF spectra, respectively. The squares, circles, and diamonds correspond

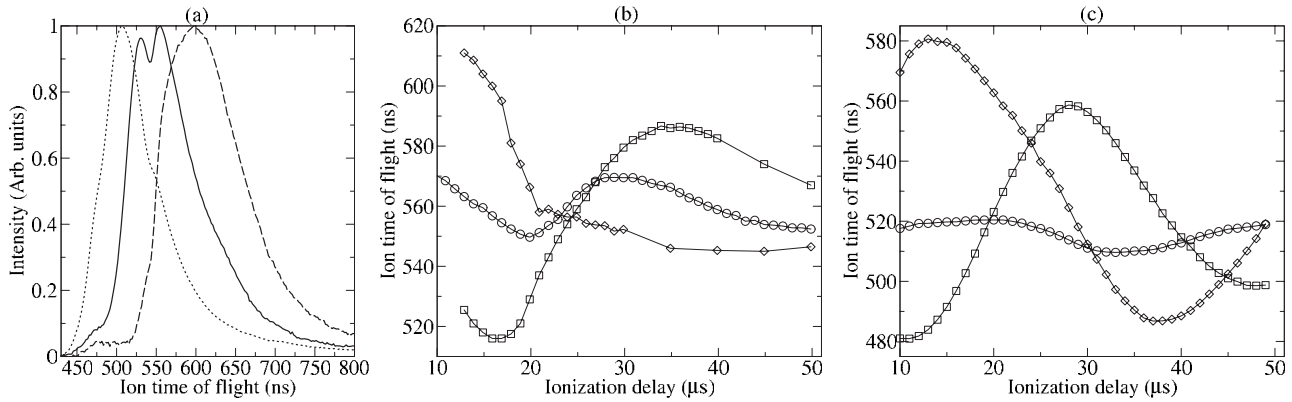

FIG. 4. (a) Ion time of flight for an ionization delay of 13.1 μs. (b), and (c) Average ion time of flight as a function of the ionization delay taken from the experimental and simulated traces, respectively. The squares, circles, and diamonds correspond to measurements carried out with V_{decel}=1375, 1155, and 935 V, respectively. The relative uncertainty in the average times of flight amounts to ~5 ns.

to measurements carried out with V_{decel}=1375, 1155, and 935 V, respectively. The average ion times of flight are smaller by ~40 ns in the simulations than in the experiments, primarily because of the finite response time of the detector which was not taken into account in the simulations. Both the simulations and the experiment show clear oscillations in the average ion TOF that reflect oscillations in the position of the atom cloud and reveal a restoring force toward the center of the trap. The particles are thus truly trapped in the z dimension. In the experiment the amplitudes of the oscillations diminish faster than in the simulations. This is probably caused by the facts that several k states are excited and that the initial particle distributions are not exactly Gaussian. To first approximation, the oscillation period (~40 μs) corresponds to twice the time it takes for the atoms to move from one side of the trap to the other, a conclusion that is confirmed by the simulations. Measurements such as those displayed in Fig. 4 represent a convenient way of determining and optimizing the position of the atom cloud in the trap.

C. n and k acceptance of the trap

Figure 5 shows a spectrum obtained by exciting the atoms to Rydberg-Stark states in the range n=24–34 using V_{trap}^{12}=45 V and V_{trap}^{34}=25 V, which corresponds to an electric field at the excitation point of approximately 100 V/cm, decelerating and trapping the atoms using V_{decel}=1155 V, and field ionizing them after a delay of 50 μs. Only blueshifted Stark states can be decelerated and trapped in this way. The figure reveals that Rydberg atoms over a relatively broad n distribution can be trapped using a single set of deceleration and trapping voltages. At each n value several Stark states contribute to the detected signal. A quantitative reconstruction of the exact k distribution is hindered by the fact that the inhomogeneous line broadening and the finite laser bandwidth prevent the resolution of the Stark structure. Nevertheless, comparison with simulations suggest that the $k \gtrsim 15$ Stark levels contribute at n=24 and the $k \gtrsim 10$ levels at n=34. The wide range of n and k values of the trapped atoms is a consequence of the large dimension of the trap (radius ~2 mm) compared to the deceleration distance (also ~2 mm). By slightly changing the potentials, we were able to optimize the trapping for different ranges of n values from below n=20 to beyond n=40.

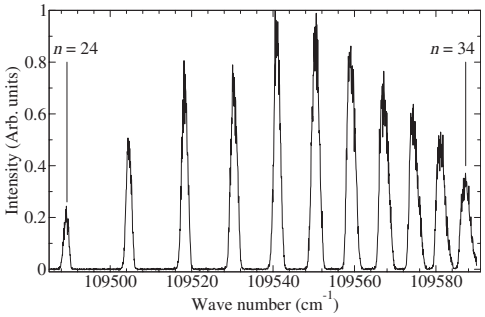

FIG. 5. Spectra of the deceleration and trapping efficiency during the first 50 μs for n=24–34. The potentials that were used are V_{trap}^{12}=45 V, V_{trap}^{34}=25 V, and V_{decel}=1155 V. The intensity of the strongest line (n=28) has been normalized to 1.

The results displayed in Fig. 5 are relevant to experiments on antihydrogen ($\bar{\mathrm{H}}$). To reach a certain degree of state selectivity in $\bar{\mathrm{H}}$ production it has been proposed to synthesize antihydrogen by resonant positron transfer from a Rydberg state of positronium [20]. Calculations [21] suggest that $\bar{\mathrm{H}}$ is produced over a range of several n and k values. The ability to trap Rydberg atoms with different n and k values illustrated in Fig. 5 implies that a significant fraction of the $\bar{\mathrm{H}}$ could be trapped, irrespective of the range of n values under consideration.

IV. CONCLUSIONS

Compared to the magnetic Rydberg atom trap recently demonstrated in Ref. [7], the present electrostatic trap offers the advantage that Rydberg atoms in well-defined n and k states are trapped, but the disadvantage of shorter trapping times. The trap is very versatile and Rydberg atoms with different n and k values can be trapped, the redistribution of n and k values induced by blackbody radiation does not lead

to significant trap losses under our experimental conditions.

The analysis of the time dependence of the signal losses reveals four contributions of different origins. (i) Signal losses resulting from the nonzero velocity in the untrapped (x) dimension are unavoidable at long times. They can be, and have been, modelled and corrected for using information contained in direct measurements of the velocity distribution by imaging techniques. (ii) At short times, i.e., $\leqslant 75$ μs, when a substantial fraction of the Rydberg atoms are still located close to the supersonic beam propagation axis, the undecelerated argon atoms in the trailing part of the gas pulse knock a fraction of the H atoms out of the trap. This effect, which is noticeable but not dominant at low nozzle stagnation pressures, becomes more and more important with increasing nozzle stagnation pressure. (iii) Beyond ≈ 75 μs, when the atom cloud has moved away from the supersonic beam, collisions with the thermalized background gas are noticeable but only make a very small contribution to the trap losses, especially in measurements carried out at nozzle stagnation pressures below 2 bars. (iv) The main source of trap losses beyond 75 μs is the fluorescence of the Rydberg atoms to lower, untrapped n states.

The investigation of the velocity and spatial distributions of the trapped atoms show that translational temperature at equilibrium amounts to ≈ 350 mK. The density of trapped atoms is initially $\approx 5 \times 10^6$ cm^{-3} when a nozzle stagnation pressure of 1.5 bars is used and decreases exponentially with a $1/e$ decay time of the order of 150 μs. Larger densities are obtained when higher nozzle stagnation pressures are used; however, in this case the trapping times decrease because of an increasingly important role played by collisions.

Because all atoms and molecules possess Rydberg states the present results establish a new, general procedure to trap a wide variety of species.

ACKNOWLEDGMENTS

We thank René Gunzinger for his help in the construction of the trap. This work was supported financially by ETH Zurich (including Q-SIT) and the Swiss National Science Foundation under project 200021-113886.

[1] K. Singer, M. Reetz-Lamour, T. Amthor, L. G. Marcassa, and M. Weidemüller, Phys. Rev. Lett. **93**, 163001 (2004).
[2] D. Tong, S. M. Farooqi, J. Stanajevic, S. Krishnan, Y. P. Zhang, R. Cote, E. E. Eyler, and P. L. Gould, Phys. Rev. Lett. **93**, 063001 (2004).
[3] T. Vogt, M. Viteau, J. Zhao, A. Chotia, D. Comparat, and P. Pillet, Phys. Rev. Lett. **97**, 083003 (2006).
[4] M. P. Robinson, B. Laburthe Tolra, M. W. Noel, T. F. Gallagher, and P. Pillet, Phys. Rev. Lett. **85**, 4466 (2000).
[5] W. Li, P. J. Tanner, and T. F. Gallagher, Phys. Rev. Lett. **94**, 173001 (2005).
[6] M. D. Lukin, M. Fleischhauer, R. Cote, L. M. Duan, D. Jaksch, J. I. Cirac, and P. Zoller, Phys. Rev. Lett. **87**, 037901 (2001).
[7] J. H. Choi, J. R. Guest, A. P. Povilus, E. Hansis, and G. Raithel, Phys. Rev. Lett. **95**, 243001 (2005).
[8] T. Breeden and H. Metcalf, Phys. Rev. Lett. **47**, 1726 (1981).
[9] W. H. Wing, Phys. Rev. Lett. **45**, 631 (1980).
[10] D. Townsend, A. L. Goodgame, S. R. Procter, S. R. Mackenzie, and T. P. Softley, J. Phys. B **34**, 439 (2001).
[11] S. R. Procter, Y. Yamakita, F. Merkt, and T. P. Softley, Chem. Phys. Lett. **374**, 667 (2003).
[12] E. Vliegen, H. J. Wörner, T. P. Softley, and F. Merkt, Phys. Rev. Lett. **92**, 033005 (2004).
[13] E. Vliegen and F. Merkt, J. Phys. B **38**, 1623 (2005).
[14] E. Vliegen and F. Merkt, J. Phys. B **39**, L241 (2006).
[15] E. Vliegen and F. Merkt, Phys. Rev. Lett. **97**, 033002 (2006).
[16] T. F. Gallagher, *Rydberg Atoms* (Cambridge University Press, Cambridge, England, 1994).
[17] E. Vliegen, P. Limacher, and F. Merkt, Eur. Phys. J. D **40**, 73 (2006).
[18] H. A. Bethe and E. E. Salpeter, *Quantum Mechanics of One- and Two-electron Atoms* (Springer, Berlin, 1957).
[19] E. J. Galvez, C. W. MacGregor, B. Chaudhuri, S. Gupta, E. Massoni, and F. DeZela, Phys. Rev. A **55**, 3002 (1997).
[20] G. Gabrielse, Adv. At., Mol., Opt. Phys. **50**, 155 (2005).
[21] M. L. Wall, C. S. Norton, and F. Robicheaux, Phys. Rev. A **72**, 052702 (2005).